NANO LETTERS

Letter

pubs.acs.org/NanoLett

Carbon Nanotube Quantum Dots As Highly Sensitive Terahertz-Cooled Spectrometers.

M. Rinzan,[†] G. Jenkins,[‡] H. D. Drew,[‡] S. Shafranjuk,[§] and P. Barbara*[,†]

[†]Department of Physics, Georgetown University, Washington, D.C. 20057, United States

[‡]Department of Physics, University of Maryland, College Park, Maryland 20742, United States

[§]Department of Physics and Astronomy, Northwestern University, Evanston, Illinois 60208, United States

Supporting Information

ABSTRACT: Terahertz technology has recently emerged as a highly sought-after and versatile scientific tool in many fields, including medical imaging, security screening, and wireless communication. However, scientific progress has been hindered by the lack of sources and detectors in this frequency range, thereby known as the terahertz gap. Here, we show that carbon nanotube quantum dots coupled to antennas are extremely sensitive, broad-band, terahertz quantum detectors with spectral resolution. Their response is due to photon-assisted single-electron tunneling and it is substantially enhanced by a novel radiation-induced nonequilibrium cooling of the electrons, causing a sharp height increase of the Coulomb oscillation peaks.

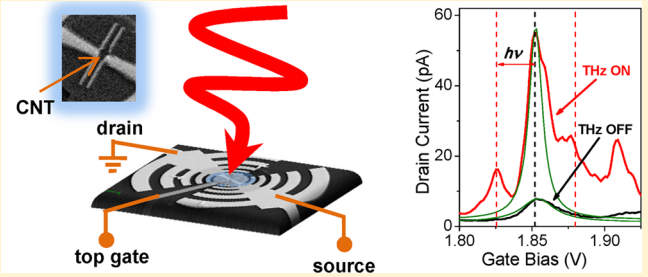

KEYWORDS: *Carbon nanotubes, quantum dots, terahertz detectors, nonequilibrium cooling, photon-assisted tunneling*

A carbon nanotube quantum dot (CNT-Dot) is a small section of CNT connecting two weakly coupled source (S) and drain (D) electrodes,[1] capacitively coupled to a third gate electrode. The total capacitance of the CNT section, C_{tot}, determines the charging energy $\delta = e^2/C_{tot}$ that is needed to add a single electron to the dot. When $\delta > kT$, the source–drain conductance shows peaks as a function of gate voltage, corresponding to resonant elastic tunneling of electrons through the dot one by one; Coulomb blockade occurs between the peaks and the voltage interval between the peaks is characterized by the energy level spacing ΔE and the charging energy of the dot.[1] When electromagnetic radiation is present, photon-assisted single-electron tunneling (PASET) (inelastic tunneling with absorption and emission of photons) is expected to change the current versus gate voltage curve and create satellite peaks with amplitudes determined by the field intensity and voltage spacing from the main peak is proportional to the photon energy.[2,3] Therefore, unlike conventional bolometric sensors[4,5] or sensors based on nonlinearity of the current voltage characteristics,[6−8] PASET sensors can determine both the intensity and the frequency of the radiation. More importantly, a CNT-Dot can operate as a wide band spectrometer from a few hundred gigahertz up to frequencies corresponding to photon energy $hf \simeq \delta$, which is on the order of 10 meV (2.5 THz) or larger.

Kawano et al.[9,10] recently demonstrated detection at terahertz frequencies via photon-assisted tunneling with power coupled to the CNT-Dot in the femtowatt range. Notwithstanding this report of successful detection, the experiment clearly presented two main challenges that hampered further research. The first was the small coupling between the detector and the 10 mW laser source. The second was the difficulty to reproduce the results on multiple samples.

Here we implement a novel design with a local top gate for each device, where the terahertz radiation is efficiently coupled to CNT-Dots through broad band on-chip antennas forming the source and drain electrodes. With this new design, we achieved a very strong and broad band response from much weaker sources (power smaller than 10 μW). This substantially improved coupling also unveiled new features that are not predicted by orthodox photon-assisted tunneling models. In addition to the satellite peaks on the left and right side of the main peaks, an anomalous height increase and sharpening of the main peak also occurs, leading to the counterintuitive conclusion that the effective electron temperature is decreased by the terahertz irradiation.

Our CNT-Dot devices were grown by chemical vapor deposition on undoped Si substrates capped by 1500 nm thick thermally grown SiO_2. Titanium source and drain electrodes were patterned by e-beam lithography as log-periodic broad-band antennas, shown in Figure 1b, with lower and upper threshold frequencies of 680 GHz and 2.5 THz, respectively. The gate dielectric was obtained by cross-linking 200 nm thick PMMA and the top gate by sputtering a Cr/Au layer, as shown in Figure 1a. The measurements were done in an optical

Received: March 11, 2012
Revised: May 21, 2012
Published: May 25, 2012

   dx.doi.org/10.1021/nl300975h | *Nano Lett.* 2012, 12, 3097−3100

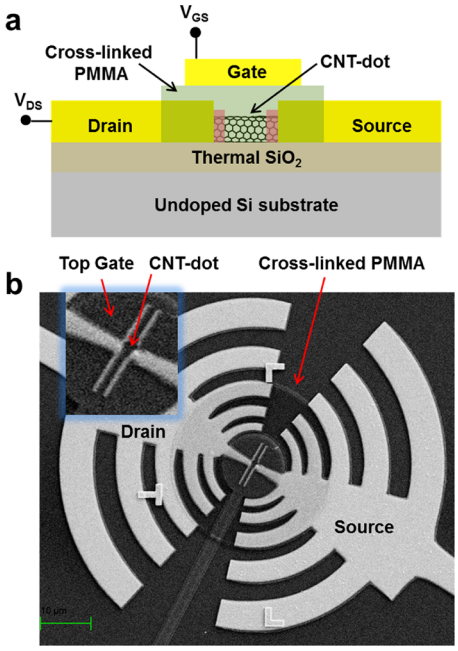

Figure 1. Schematic diagram and image of the carbon nanotube quantum dot (CNT-Dot) sensors. (a) Cross-section of the CNT-Dot device structure. (b) Scanning electron microscope image of a device. Inset: Zoom-in of the quantum dot region. In the design, the source and drain electrodes are separated by 400 nm, corresponding to energy level spacing $\Delta E \approx 4$ meV. The carbon nanotube connecting the electrodes cannot be distinguished due to the PMMA gate dielectric deposited on top of it.

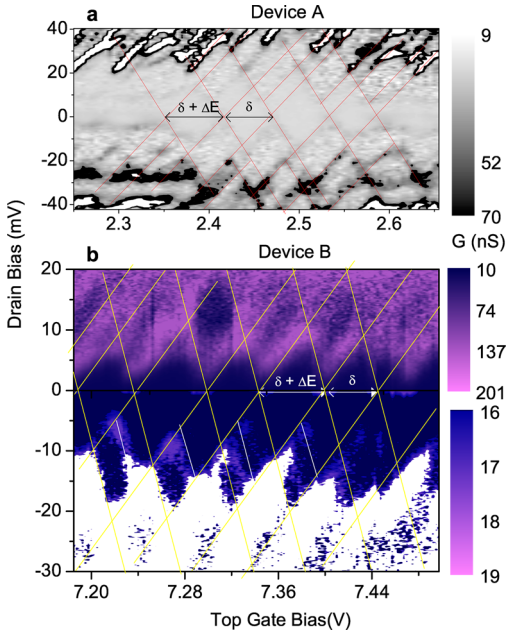

Figure 2. Quantum dot characterization. (a) Differential conductance as a function of gate voltage and source−drain bias for device A. (b) Similar characterization for device B: The current versus drain bias for device B was quite asymmetric, therefore we used two different color scales for positive and negative source−drain bias to reveal the diamond pattern clearly. The lines running parallel to the edges of the coulomb blockade diamonds correspond to excited levels. The slopes of the diamonds were used to extract the quantum dot characteristic parameters. The charging energy for sensor A (B) is δ = 13.7 (7.4) meV. The source and drain capacitances are C_S = 3.7 (11.8) aF and C_D = 4.4 (6.1) aF, the gate capacitance C_G = 3.6 (3.8) aF and the energy level spacing is ΔE = 3.3 (1.9) meV.

cryostat and a Winston cone was used to focus the radiation on the sample.

We present results on two devices, A and B. Both devices showed Coulomb blockade oscillations below 10 K. The differential conductance as a function of gate voltage and drain bias for these devices is plotted as color maps in Figure 2. Both devices exhibit typical Coulomb blockade diamonds, but these features are not as sharp as those usually obtained for CNT-Dots in the standard back-gate configuration, with silicon dioxide as a gate dielectric. However, they are still sufficiently well-defined to extract the characteristic quantum-dot parameters, including the charging energy δ, and the single particle level spacing ΔE for each device (see Figure 2). The lines running parallel to the edges of diamonds correspond to tunneling of carriers through excited states of the CNT-Dots.

The devices were irradiated using two different sources: a backward wave oscillator (BWO) with frequency continuously tunable from 680 to 1080 GHz and a CO_2 pumped gas laser at a fixed frequency of 1.27 THz. The response of device A irradiated by the BWO at different frequencies is shown in Figure 3a. Since in this sample the width of the Coulomb blockade peak is comparable to the photon energy, the satellite peaks do not resolve into separate peaks. Instead, they are merged with the main peak to form a wider peak. Such widening can in fact be measured at all frequencies and it increases with increasing frequency. Notably, in addition to the peak widening, we also measure a strong enhancement of the main peak, especially at frequencies above 800 GHz, corresponding to photon energy larger than ΔE for this device. In device B, the Coulomb peaks are narrower, therefore, the PASET satellite peaks can be clearly distinguished, as shown in Figure 3b,c. As expected for photon-assisted tunneling, the height of the side peaks increases when the source intensity increases, and the voltage spacing of the side peaks increases proportionally to the photon energy. The factor of proportionality is the gate efficiency of the device, $\alpha_G = C_G/C_{tot} \simeq 18\%$, where C_G is the gate capacitance.

Also in device B, when the source intensity increases, both the height of the side peak and the height of the main peak increase. This result is quite remarkable because according to orthodox photon-assisted tunneling theory[11] the height of the main peak is expected to decrease when the radiation intensity is increased. We note that the height increase of the main peak measured in devices A and B is clearly not due to heating. Figure 3d shows the temperature dependence of the Coulomb blockade peaks, when no radiation is applied. The Coulomb blockade peaks broaden and their height decreases when the temperature is increased, whereas they become narrower and their height increases upon shining terahertz radiation.

To understand this anomalous increase of the Coulomb blockade peak, an important amendment to the standard PASET model[2,12] is considered. We account for nonequilibrium effects in the CNT-Dot and compute the nonequilibrium electron distribution function $g(\varepsilon_k)$ from solutions of the quantum kinetic equation.[13] We assume that the tunneling rates $\Gamma_{S,D}$ through source−dot and dot−drain Schottky barriers are energy dependent and model $\Gamma_D(\varepsilon_k)$ as $\Gamma_D(\varepsilon_k) = \Gamma_D^{(0)}(\varepsilon_k/\delta)^{1/2}$ while $\Gamma_S \equiv$ const[2,12] with $\Gamma_{S,D} \ll \delta$.

Figure 4 shows the computed drain current as a function of gate voltage with different field intensities (Figure 4a) and frequencies (Figure 4b). The curves show distinct satellite

dx.doi.org/10.1021/nl300975h | Nano Lett. 2012, 12, 3097−3100

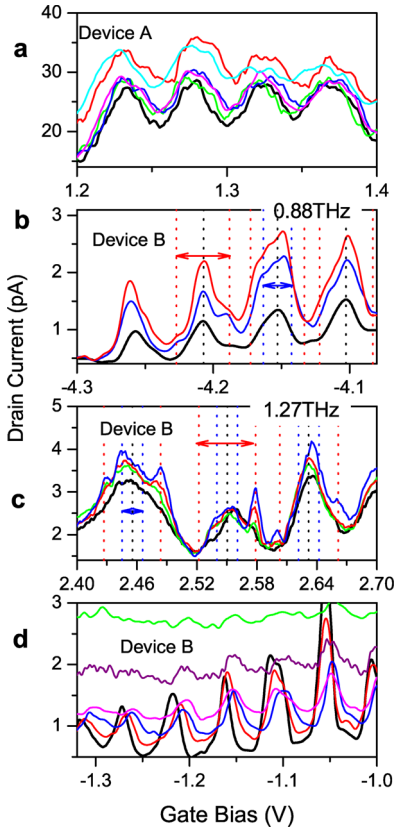

Figure 3. Terahertz response and temperature dependence of Coulomb blockade peaks. (a) Device A irradiated with the BWO source at different frequencies, corresponding to hf = 2.83 (green), 3.19 (pink), 3.65 (blue), 4.05 (cyan), and 4.46 (red) meV. The black curve in panels a through c represents dark current (THz off). (b) Device B irradiated with the BWO source (hf = 3.63 meV) with increasing power from low (blue) to high (red). The red vertical lines show positions of satellite peaks due to PASET with spacing $2hf/\alpha_G$ indicated by the red arrow. The blue vertical lines correspond to pronounced transport through excited states with spacing $2\Delta E/\alpha_G$ (ΔE = 1.9 meV), indicated by the blue arrow. (c) Device B irradiated with the laser source (hf = 5.24 meV) with increasing power from low (blue) to high (red). (d) Device B without any terahertz irradiation at different temperatures, 2.5 (black curve with tall peaks), 8, 10, 12, 14, and 16 K (flat, green curve above 2.5 pA).

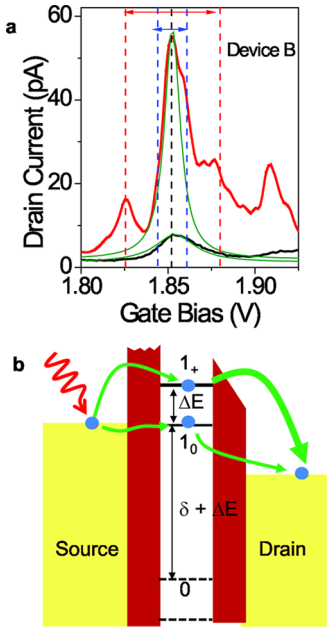

Figure 5. (a) Measured response of device B to the laser source with frequency corresponding to hf = 5.24 meV (red curve). The black curve shows the dark current of the terahertz sensor. The green curves are Lorentzian fits to the terahertz and dark Coulomb blockade peaks with widths of 11 and 28 mV, respectively. The red vertical lines show positions of satellite peaks due to PASET with spacing $2hf/\alpha_G$ indicated by the red arrow and the blue vertical lines correspond to pronounced transport through excited states with spacing $2\Delta E/\alpha_G$ (ΔE = 1.9 meV), indicated by the blue arrow. (b) Schematic diagram of electron tunneling processes through the CNT-Dot. For terahertz frequencies corresponding to $hf < \Delta E$, electrons tunnel from the source to the drain through level 1_0. At higher frequencies, $hf > \Delta E$, photon-assisted tunneling occurs through the excited level 1_+. If the tunneling rate from the dot to the drain electrode Γ_D increases when increasing the electron energy, then $\Gamma_D(E_{1+}) > \Gamma_D(E_{10})$ and the most energetic electrons leave the dot at a faster rate, causing the effective temperature of the electrons in the dot to decrease.

peaks with spacing from the main peak proportional to the photon energy. Similarly to the experimental data, they also clearly show the anomalous increase of the main peak when either the field intensity or the frequency is increased. We assume that the crystal temperature of the dot is in equilibrium

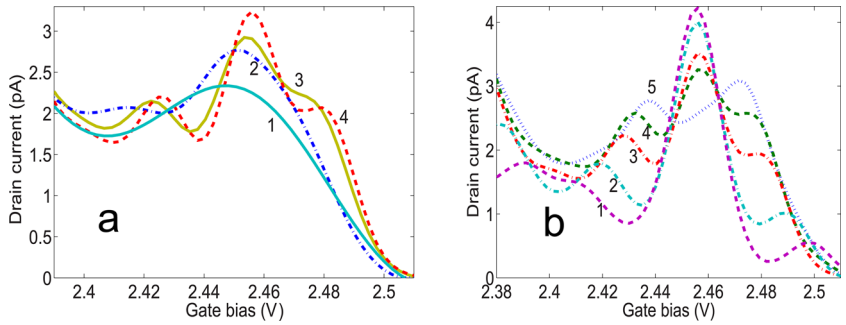

Figure 4. Frequency and amplitude dependence of computed current versus gate voltage. (a) Fixed frequency, hf = 5.25 meV, and different values of $\tilde{V}_S$ = 0, 3.4, 4.4, and 5.5 mV for curves 1, 2, 3 and 4, respectively, where $\tilde{V}_S$ ($\tilde{V}_D$) is the amplitude of the ac voltage drop across the source−dot (dot−drain) barrier and $\tilde{V}_D$ = 0.55 $\tilde{V}_S$. Curves 2−4 correspond to effective electron temperature T^*_{2-4} = 6.9, 5.25, and 4.2 K. The "dark current", curve 1, corresponds to T^*_1 = 9.3 K. (b) Different frequencies, hf = 7.31, 6.33, 4.67, 3.31, and 3.02 meV for curves 1−5, respectively, at $\tilde{V}_S$ = 5.2 mV. Curves 1−5 correspond to effective electron temperatures T^*_{1-5} = 4.5, 4.7, 4.95, 5.15, and 6.6 K, respectively. The dot/drain tunneling rate parameter $\Gamma_D^{(0)}$ = 0.6 meV. Both graphs illustrate terahertz cooling of the dot.

dx.doi.org/10.1021/nl300975h | Nano Lett. 2012, 12, 3097−3100

with the source and drain electrodes and compute the effective electron temperature (T^*) in the dot. The effective temperature is obtained by balancing the energy gain of the dot due to the terahertz field and electrons tunneling into the dot from the source electrode and the energy loss due to electrons tunneling from the dot to the drain electrode. We find that T^* decreases with increasing frequency.

The model sketched in Figure 5 explains this nontrivial behavior as caused by nonequilibrium cooling of the quantum dot, when the terahertz frequency is sufficiently high. If the frequency $hf < \Delta E$, electrons populate mainly level 1_0, whereas, if $hf \geq \Delta E$, also the upper 1_+ level is populated. Because the tunneling rate $\Gamma_D(\varepsilon_k)$ is higher at $\varepsilon_k \simeq E_{1+}$, $\Gamma_D(E_{1+}) \gg \Gamma_D(E_{10})$, electrons on level 1_+ escape to the drain electrode much faster than they did from level 1_0 (as indicated by the thicker arrow in Figure 5). The removal of the "hottest" electrons at a higher rate for $hf \geq \Delta E$ decreases the effective electron temperature in the dot, leading to the height increase and the width decrease of the Coulomb peak. Although additional features due to transport through excited states (see blue vertical lines) are also enhanced and appear as shoulders on the main peak, the reduced width of the Coulomb blockade peaks under terahertz irradiation can be clearly observed from the Lorentzian fits (green curves) in Figure 5a.

We show that CNT-Dots are extremely sensitive quantum detectors and potential building blocks for terahertz (submillimeter) spectrometers. The anomalous strongly enhanced response due to nonequilibrium cooling opens the way to novel approaches for higher temperature operation, which is highly desirable for practical applications. Further research will focus on increasing the nonequilibrium cooling effects by optimizing the CNT-Dot characteristic parameters.

■ ASSOCIATED CONTENT

Ⓢ Supporting Information

Details on the model and the simulations are available. This material is available free of charge via the Internet at http://pubs.acs.org.

■ AUTHOR INFORMATION

Corresponding Author

*E-mail: barbara@physics.georgetown.edu.

Notes

The authors declare no competing financial interest.

■ ACKNOWLEDGMENTS

This work was supported by AFOSR Grants FA9550-09-1-0697 and FA9550-09-1-0685. H.D.D. and G.J. acknowledge support from DOE Grant DE-SC0005436.

■ REFERENCES

(1) Tans, S. J.; Devoret, M. H.; Dai, H.; Thess, A.; Smalley, R. E.; Geerligs, L. J.; Dekker, C. Individual single-wall carbon nanotubes as quantum wires. *Nature* **1997**, *386*, 474−477.

(2) Kouwenhoven, L. P.; Jauhar, S.; Orenstein, J.; McEuen, P. L.; Nagamune, Y.; Motohisa, J.; Sakaki, H. Observation of photon assisted tunneling through a quantum dot. *Phys. Rev. Lett.* **1994**, *73*, 3443−3446.

(3) Meyer, C.; Elzerman, J. M.; Kouwenhoven, L. P. Photon-Assisted Tunneling in a Carbon Nanotube Quantum Dot. *Nano Lett.* **2007**, *7*, 295−299.

(4) Fu, K.; Zannoni, R.; Chan, C.; Adams, S. H.; Nicholson, J.; Polizzi, E.; Yngvesson, K. S. Terahertz detection in single wall carbon nanotubes. *Appl. Phys. Lett.* **2008**, *92*, 033105−033107.

(5) Santavicca, D. F.; Chudow, J. D.; Prober, D. E.; Purewal, M. S.; Kim, P. Bolometric and nonbolometric radio frequency detection in a metallic single-walled carbon nanotube. *Appl. Phys. Lett.* **2011**, *98*, 223503−223505.

(6) Chudow, J. D.; Santavicca, D. F.; McKitterick, C. B.; Prober, D. E.; Kim, P. Terahertz detection mechanism and contact capacitance of individual metallic single-walled carbon nanotubes. *Appl. Phys. Lett.* **2012**, *100*, 163503−163507.

(7) Vitiello, M. S.; Coquillat, D.; Viti, L.; Ercolani, D.; Teppe, F.; Pitanti, A.; Beltram, F.; Sorba, L.; Knap, W.; Tredicucci, A. Room-Temperature Terahertz Detectors Based on Semiconductor Nanowire Field-Effect Transistors. *Nano Lett.* **2012**, *12*, 96−101.

(8) Vicarelli, L.; Vitiello, M. S.; Coquillat, D.; Lombardo, A.; Ferrari, A. C.; Knap, W.; Polini, M.; Pellegrini, V.; Tredicucci, A. Graphene field effect transistors as room-temperature terahertz detectors. arXiv:1203.3232v1.

(9) Fuse, T.; Kawano, Y.; Yamaguchi, T.; Aoyagi, Y.; Ishibashi, K. Quantum response of carbon nanotube quantum dots to terahertz wave irradiation. *Nanotechnology* **2007**, *18*, 044001.

(10) Kawano, Y.; Fuse, T.; Toykawa, S.; Uchida, T.; Ishibashi, K. Terahertz photon-assisted tunneling in carbon nanotube quantum dots. *J. Appl. Phys.* **2008**, *103*, 034306−034309.

(11) Tien, P. K.; Gordon, J. P. Multiphoton process observed in the interaction of microwave fields with the tunneling between superconductor films. *Phys. Rev.* **1963**, *129*, 647−651.

(12) Averin, D.; Korotkov, A. N.; Likharev, K. K. Theory of single-electron charging of quantum wells and dots. *Phys. Rev. B* **1991**, *44*, 6199−6211.

(13) Keldysh, L. V. Diagram technique for non-equilibrium processes. *Sov. Phys. JETP* **1965**, *20*, 1018−1023.